Mon. Not. R. Astron. Soc. **365,** 1149–1159 (2006) doi:10.1111/j.1365-2966.2005.09765.x

Gamma-ray bursts as dark energy–matter probes in the context of the generalized Chaplygin gas model

O. Bertolami★ and P. T. Silva★

Instituto Superior Técnico, Departamento de Física, Avenida Rovisco Pais, 1, 1049-001, Lisboa, Portugal

Accepted 2005 October 18. Received 2005 September 21; in original form 2005 July 7

ABSTRACT

In this paper we consider the use of gamma-ray bursts (GRBs) as distance markers to study the unification of dark energy and dark matter in the context of the so-called generalized Chaplygin gas (GCG) model. We consider that the GRB luminosity may be estimated from its variability and time-lag, and we also use the so-called Ghirlanda relation. We evaluate the improvements expected once more GRBs and their redshift become available. We show that although GRBs allow for extending the Hubble diagram to higher redshifts, its use as a dark energy probe is limited when compared to Type Ia supernovae. We find that the information from GRBs can provide some bounds on the amount of dark matter and dark energy independently of the equation of state. This is particularly evident for XCDM-type models, which are, for low redshifts ($z \leqslant 2$), degenerate with the GCG.

Key words: methods: miscellaneous – cosmological parameters – cosmology: observations – dark matter – distance scale – gamma-rays: bursts.

1 INTRODUCTION

The generalized Chaplygin gas (GCG) model (Kamenshchik, Moschella & Pasquier 2001; Bento, Bertolami & Sen 2002b) is an interesting alternative to more conventional approaches for explaining the observed accelerated expansion of the Universe such as a cosmological constant (see, for example, Bento & Bertolami 1999; Bento, Bertolami & Silva 2001) or quintessence (Ratra & Peebles 1988a,b; Wetterich 1988; Caldwell, Dave & Steinhardt 1998; Ferreira & Joyce 1998; Amendola 1999; Binétruy 1999; Chiba 1999; Uzan 1999; Zlatev, Wang & Steinhardt 1999; Albrecht & Skordis 2000; Bertolami & Martins 2000; Kim 2000; Sen, Sen & Sethi 2001; Sen & Sen 2001; Bento, Bertolami & Santos 2002a). It is worth remarking that quintessence is related to the idea that the cosmological term could evolve (Bronstein 1933; Bertolami 1986a,b; Ozer & Taha 1987) and to attempts to solve the cosmological constant problem.

In the GCG approach, an exotic equation of state is considered to describe the behaviour of the background fluid

$$p_{\rm ch} = -\frac{A}{\rho_{\rm ch}^{\alpha}}, \tag{1}$$

where A and α are positive constants. The case $\alpha = 1$ corresponds to the Chaplygin gas. In most phenomenological studies the range $0 < \alpha \leqslant 1$ is considered. Within the framework of Friedmann–Robertson–Walker cosmology, after being inserted into the relativistic energy conservation equation, this equation of state leads to an evolution of the energy density as (Bento et al. 2002b)

$$\rho_{\rm ch} = \left[A + \frac{B}{a^{3(1+\alpha)}}\right]^{1/(1+\alpha)}, \tag{2}$$

where a is the scale factor of the Universe and B is a positive integration constant. From this result, we can understand a striking property of the GCG: at early times the energy density behaves as matter while at late times it behaves like a cosmological constant. This behaviour suggests the interpretation of the GCG model as an entangled mixture of dark matter and dark energy.

This model has several attractive features. From a theoretical point of view, the pure Chaplygin model ($\alpha = 1$) equation of state can be obtained from the Nambu–Goto action for d-branes moving in a $(d + 2)$-dimensional space–time in the light cone parametrization (Bordemann & Hoppe 1993). It is also the only fluid which admits a supersymmetric generalization (Jackiw & Polychronakos 2000), and also appeared in the study of the stabilization of branes in bulks with a black hole geometry (Kamenshchik, Moschella & Pasquier 2000). The Chaplygin gas may be viewed as a quintessence field with a suitable potential (Kamenshchik et al. 2001), or as an effect arising from the embedding of a $(3 + 1)$-dimensional brane in a $(4 + 1)$-dimensional bulk (Bilic, Tupper & Viollier 2002). The generalized Chaplygin gas also has a connection with brane theories (Bento et al. 2002b). The model can be yet viewed as the simplest model within the family of tachyon cosmological models (Frolov, Kofman & Starobinsky 2002).

The GCG model has also been successfully confronted with different classes of phenomenological tests: high precision cosmic microwave background radiation data (Amendola et al. 2003; Bento,

★E-mail: orfeu@cosmos.ist.utl.pt (OB); paptms@ist.utl.pt (PTS)

Bertolami & Sen 2003a,b,c; Carturan & Finelli 2003), supernova (SN) data (Fabris, Gonçalves & de Souza 2002a; Alcaniz, Jain & Dev 2003; Dev, Alcaniz & Jain 2003; Gorini, Kamenshchik & Moschella 2003; Makler, de Oliveira & Waga 2003; Bertolami et al. 2004; Zhu 2004; Bento et al. 2005) and gravitational lensing (Silva & Bertolami 2003; Dev, Jain & Alcaniz 2004). More recently, it has been shown using the latest SN data (Tonry et. al. 2003; Barris et al. 2004; Riess et al. 2004), that the GCG model is degenerate with a dark energy model with a phantom-like equation of state (Bertolami et al. 2004; Bento et al. 2005). Furthermore, it can be shown that this does not involve any violation of the dominant energy condition and hence does not lead to the big rip singularity in future (Bertolami et al. 2004). It is a feature of GCG model that it can mimic a phantom-like equation of state, but without any kind of pathologies as asymptotically the GCG approaches a well-behaved de Sitter universe. Structure formation in the context of the Chaplygin gas and the GCG was originally examined in Bento et al. (2002b), Bilic et al. (2002) and Fabris, Gonçalves & de Souza (2002b). The results of the various phenomenological tests on the GCG model are summarized in Bertolami (2004, 2005),

Subsequently, concerns about such a unified model were raised in the context of structure formation. Indeed, it has been pointed out that unphysical oscillations should be expected or even an exponential blow-up in the matter power spectrum (Sandvik et al. 2004), given the behaviour of the sound velocity through the GCG. Although, at early times, the GCG behaves like dark matter and its sound velocity is vanishingly small, at later times the GCG starts behaving like dark energy with a substantial negative pressure, yielding a large sound velocity which, in turn, can produce oscillations or blow-up in the power spectrum. This is a common feature of any unified approach when the dark matter and the dark energy components of the fluid are not clearly identified. These components are, of course, interacting, as they make part of the same fluid. It can be shown however that the GCG is a unique mixture of interacting dark matter and a cosmological constant-like dark energy, once the possibility of phantom-type dark energy is excluded (Bento, Bertolami & Sen 2004). It can be shown that as a result of the interaction between the components, there is a flow of energy from dark matter to dark energy. This energy transfer is not significant until the recent past, resulting in a negligible contribution at the time of gravitational collapse ($z_c \simeq 10$). Subsequently, at about $z \simeq 0.2$, the interaction starts to grow, yielding a large energy transfer from dark matter to dark energy, which leads to the dominance of the latter at present. Actually, it is shown that the epoch of dark energy dominance occurs when dark matter perturbations start deviating from its linear behaviour and that the Newtonian equations for small-scale perturbations for dark matter do not involve any mode-dependent term. Thus, neither oscillations nor blow-up in the power spectrum do develop.

In this paper we study yet another cosmological test and its possible use to study the GCG. Schaefer (2003) suggested that gamma-ray bursts (GRBs) may be used to extend the Hubble diagram to redshifts as high as $z \sim 5$. For 'ordinary' dark energy, such high redshifts are not very interesting because at those epochs the Universe is dominated by dark matter, and thus it is less sensitive to the nature of dark energy.

For the GCG however, the GRB test might be relevant because it unifies dark energy and dark matter into one single fluid. Therefore, within the framework of the GCG model, the dark matter domination period actually depends of the nature of the dark energy component that kicks in at later times, and we can expect that the study of the matter-dominated era will bring some insight into some properties of GCG models.

This paper is organized as follows. In Section 2 we explain our method of using the time-lag/luminosity and variability/luminosity correlations to constrain cosmological models. In Section 3 we present and comment on the results obtain from this method. In Section 4 we consider a more precise correlation found by Ghirlanda, Ghisellini & Lazzati (2004a), and study its consequences. In Section 5 we consider whether it is possible to use the extended redshift range of GRBs to break the degeneracy between the GCG and the XCDM (cold dark matter plus a dark energy component with a constant equation of state). Finally, in Section 6 we discuss our results and present our conclusions.

2 METHOD

2.1 Overview

The starting point of our study is the proposed correlation between time-lags in GRBs spectra and the isotropic equivalent luminosity (Norris, Marani & Bonnell 2000), and the correlation between GRB variability and isotropic equivalent luminosity (Reichart et al. 2001). The time-lag, denoted by $\tau_{\rm lag}$, measures the time offset between high- and low-energy GRB photons that arrive on Earth. The variability, V, is easily defined in qualitative terms as a measurement of the 'spikiness' or complexity of the GRB light curve. The isotropic equivalent luminosity is the inferred luminosity of a GRB if all its energy is radiated isotropically. That is, if P is the peak flux of a burst in units of photons cm^{-2} s^{-1} between observer frame energies $E_{\rm l}$ and $E_{\rm u}$, the isotropic equivalent peak photon luminosity of the burst in erg s^{-1} in the source frame energy range 30 to 2000 keV is given by

$$L_{\rm iso} = 4\pi r^2(z) P \frac{\int_{30}^{2000} E N(E)\,{\rm d}E}{\int_{E_{\rm l}(1+z)}^{E_{\rm u}(1+z)} N(E)\,{\rm d}E} \qquad (3)$$

where $N(E)$ is the source frame spectral shape, usually parametrized by a Band function (Band et al. 1993), and $r(z)$ is the comoving distance to a burst at redshift z.

The possible use of this relation to expand the Hubble diagram to higher redshifts was first discussed in Schaefer (2003). One limitation of the employed method is the cosmological distances of GRBs, which affect the ability of performing a proper calibration of their distance independently of the background cosmology. It is necessary either to fix a cosmological model and find a calibration that depends on the assumed cosmological model, or to fit the data to both calibration and cosmological parameters. This degrades precision because there are more free parameters for the same number of data points.

One way around this was proposed by Takahashi et al. (2003). Let us assume that we measure the luminosity distance up to $z = z_{\rm max}$, with say $z_{\rm max} = 1.5$. This is, for instance, very likely to be possible with the *Supernova Acceleration Probe* (*SNAP*)[1] mission. This means that we would have an estimate of the absolute isotropic luminosity that is independent of the calibration and of the cosmological model. We can then use these estimates to calibrate the ($\tau_{\rm lag}$, $L_{\rm iso}$) and (V, $L_{\rm iso}$) relations without assuming a background cosmological model.

The major strength of GRBs as cosmological probes is that they can be found at very high redshifts (Lamb & Reichart 2000). We can then use high-redshift GRB data to probe the cosmology. This is

[1] See http://snap.lbl.gov/.

done by using the $(\tau_{\rm lag}, L_{\rm iso})$ and $(V, L_{\rm iso})$ relations to estimate the luminosity distance at higher redshifts. A possible method would be to use GRBs with $z < 1.5$ together with the luminosity distance estimates from SNe to calibrate the luminosity estimator, and then use this calibration to find the luminosity distance of GRBs with $z > 1.5$. It should be noted that this method aims to study the luminosity distance in the range $1.5 < z < 5$. Later, it will be shown that adding information obtained in the range $z < 1.5$ is actually crucial to the study of dark energy models.

With this information, we can estimate the luminosity distance at high redshifts, and place constraints on the cosmological parameters via a standard χ^2 minimization procedure.

The aim of this paper is to use this method to constrain the GCG unification model of dark energy and dark matter. Even though it is shown that the optimum redshift range for studying dark energy is around $z < 2$ (Huterer & Turner 2001), as already remarked, because the GCG also describes dark matter, a higher redshift range might be relevant for a better understanding of the model.

Our study is performed in three steps. First, we build a realistic mock distribution of GRBs in redshift and isotropic luminosity space (Section 2.2). Secondly, we test the calibration procedure to find what improvements might be achieved in the future. To do this, we consider a fiducial set of calibration parameters to generate a mock set of time-lags and variabilities for each GRB. We then perform a χ^2 fit to these mock data to study the calibration precision. The last step consists of employing this method to probe GCG models. This is done in a fashion similar to what was already performed with SNe Ia (Goliath et al. 2001; Weller & Albrecht 2002; Di Pietro & Claeskens 2003; Silva & Bertolami 2003). A fiducial cosmological model is assumed, and regions of constant χ^2 are plotted around the fiducial set of parameters.

2.2 Generating a gamma-ray burst mock population

We describe here the process of population generation. We simulate several data sets, which differ only in size. We consider three sample sizes. The first sample is composed of 150 GRBs, and is consistent with the expected number of GRBs with measured redshift $z > 1.5$, which is what the *Swift* satellite is expected to detect in its three-year mission. The second and third samples are larger, containing 500 and 1000 GRBs, respectively, and serve as best-case scenarios to test whether further data might improve the results. The GRB distribution on redshift will be part of the data generated by future GRBs surveys. Thus, our mock catalogues do not need to be extremely precise; however, they should be realistic.

The GRBs in each sample are distributed in redshift and luminosity according to the GRB rate history and luminosity function based on the model of the star formation 2 from Porciani & Madau (2001).

Denoting by $\psi(L)$ the GRB luminosity function, normalized to unity, then the observed rate of bursts with observed peak flux larger than P_1 at the redshift range $(z, z + {\rm d}z)$ is given by

$$ {\rm d}N(P \geqslant P_1) = {\rm d}z \frac{{\rm d}V(z)}{{\rm d}z} \frac{R_{\rm GRB}(z)}{1+z} \int_{L(P_1,z)}^{\infty} {\rm d}L' \psi(L') \epsilon(P). \quad (4) $$

Here $R_{\rm GRB}$ is the comoving GRB rate density, $\epsilon(P)$ is the detector efficiency as a function of photon flux, which for simplicity is assumed to be $\epsilon(P) = 1$, and $L(P, z)$ is given by equation (3).

The GRB rate is calculated assuming that it tracks the global star formation history (Porciani & Madau 2001), i.e. $R_{\rm GRB} \propto R_{\rm SF} \propto R_{\rm SN}$, where $R_{\rm SF}$ and $R_{\rm SN}$ are the comoving rate densities of star formation and core collapse (Type II) SNe.

We use the following parametrization (Steidel et al. 1999; Porciani & Madau 2001)

$$ R_{\rm SF}(z) = 0.15 h_{65} \frac{\exp(3.4z)}{\exp(3.4z) + 22} \, {\rm M}_\odot \, {\rm yr}^{-1} \, {\rm Mpc}^{-3}, \quad (5) $$

where h_{65} is the Hubble constant in units of 65 km s^{-1} Mpc^{-1}. These numerical factors were calculated for an Einstein–de Sitter universe. To convert this result into the ΛCDM model, a factor of $H(z|\Omega_{\rm m}, \Omega_\Lambda, h_{65})/H(z|1, 0, 1)$ must be introduced as a multiplication factor; here $H(z)$ is the Hubble factor as a function of redshift (see appendix A of Porciani & Madau 2001 for details).

To calculate the rate density of SNe II, it is assumed that all stars with masses $M > 8 \, {\rm M}_\odot$ explode as core-collapsed SNe. This yields an additional factor of $0.0122 \, {\rm M}_\odot^{-1}$ to be multiplied to the star formation rate. Finally, using the results obtained from Burst and Transient Source Experiment (BATSE) bursts (Porciani & Madau 2001), we have

$$ R_{\rm GRB}(z) = \frac{0.0122 h_{65}^2}{4.4 \times 10^5} \frac{H(z|\Omega_{\rm m}, \Omega_\Lambda, h_{65})}{H(z|1, 0, 1)} R_{\rm SF}(z). \quad (6) $$

We use the luminosity function (Porciani & Madau 2001)

$$ \psi(L) = C \left(\frac{L}{L_0} \right)^{\gamma} \exp\left(-\frac{L_0}{L} \right). \quad (7) $$

Here, L denotes the rest-frame peak luminosity in the 30–2000 keV energy range, and $C = [L_0 \Gamma(-\gamma - 1)]^{-1}$, where $\Gamma(x)$ is the Euler gamma function, ensures a proper normalization. Using the results from Porciani & Madau (2001) obtained for a GRB formation rate given by equation (6), we consider $\gamma = -2.9$, $L_0 = 7 \times 10^{51} \, h_{65}^{-2}$ erg s^{-1}

To calculate $L(P, z)$ we need to know the photon energy spectrum. For simplicity, we describe the energy spectrum of the GRB as a single power law with index -2.5, instead of the customary Band function (Band et al. 1993). To check whether this choice affects our results, we have calculated some mock catalogues using the Band function used in Porciani & Madau (2001). The only effect we have found was a small increase in the number of detected GRBs at very high ($z > 5$) redshifts. Because the measurement of such large redshifts is unlikely (see however Lamb & Reichart 2000), we placed an upper limit of $z \leqslant 5$ when building our samples. Thus, our results are not altered by using the Band function or the power law.

The flux limit of the *Swift* satellite, $P > 0.04$ photons cm^{-2} s^{-1}, is applied to check whether the GRB can be detected. The observed magnitude is calculated assuming a flat ΛCDM cosmological model, with $\Omega_\Lambda = 0.7$ and $H_0 = 70$ km s^{-1} Mpc^{-1}.

Because equation (4) gives us the number of GRBs that are expected to be detected in the redshift range $(z, z + {\rm d}z)$, we have that the function

$$ \phi(z, P > P_1) = {\rm d}N(z, P > P_1) \left[\int_0^{\infty} \frac{{\rm d}N}{{\rm d}z}(z, P > P_1) \, {\rm d}z \right]^{-1} \quad (8) $$

gives the probability of detecting a GRB in that redshift range. With this probability density function, we built a pseudo-random number generator to generate our mock catalogues (see, for instance, Press et al. 1992).

We show an example of a generated sample in Fig. 1.

2.3 Calibration procedure

Reichart et al. (2001) proposed a relation between the variability and isotropic equivalent luminosity of a GRB such that

$$ L_{\rm iso} = B_v V^{\beta_v}, \quad (9) $$

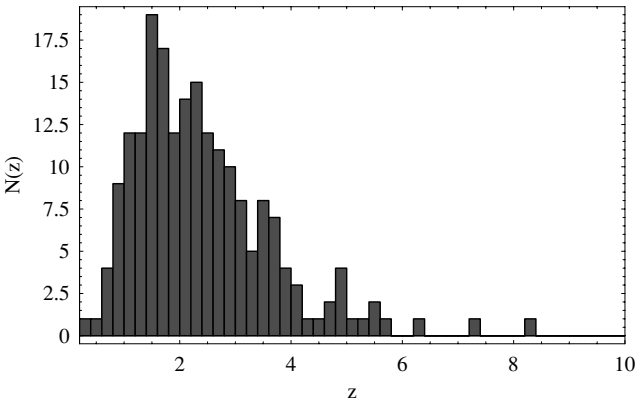

Figure 1. The redshift distribution of a GRB sample population.

while Norris et al. (2000) proposed a similar relation between $\tau_{\rm lag}$ and $L_{\rm iso}$

$$L_{\rm iso} = B_\tau \tau_{\rm lag}^{\beta_v}. \tag{10}$$

As already mentioned, the first step in testing the calibration procedure consists of establishing a fiducial model. Schaefer (2003) used the nine GRBs with available redshifts at the time to calibrate these relations, yielding

$$\beta_v = 1.57, \qquad B_v = 10^{50.03}, \tag{11}$$

$$\beta_\tau = -1.27, \qquad B_\tau = 10^{55.32}. \tag{12}$$

We assume these values as our fiducial model, i.e. we suppose that the calibration relations are faithful, and that they are described by this set of parameters. For each GRB of the mock luminosity distribution, generated as we have explained above, we compute the corresponding time-lag, $\tau_{\rm lag}$, and variability, V, using

$$\log \tau_{\rm lag} = \log B_\tau + \frac{1}{\beta_\tau} \log L + {\rm Random}(\sigma_\tau), \tag{13}$$

$$\log V = \log B_v + \frac{1}{\beta_v} \log L + {\rm Random}(\sigma_v), \tag{14}$$

where the Random (σ) term is a pseudo-random number drawn from a normal distribution with zero mean value and variance σ. That is, we assume that $\tau_{\rm lag}$ and V have lognormal error distributions, with variance σ_τ and σ_v, respectively.

The values we use for σ_v and σ_τ are based on Schaefer (2003) and are essentially dominated by an intrinsic (statistical) error. The used fiducial values are shown in Table 1.

In the real situation, we would assume that the luminosity distance at redshifts smaller than $z = 1.5$ has been measured independently by SNe Ia experiments, such as *SNAP*. Knowledge of the peak flux observed on Earth and the spectral shape $N(E)$ allow us to obtain the corresponding equivalent isotropic luminosity from equation (3).

We do not consider errors in this estimate of $L_{\rm iso}$, but it should be noted that it is expected that the luminosity distance uncertainty will be around $\sigma_{\log d_L} \sim 0.01$ for future experiments such as *SNAP* (Goliath et al. 2001; Weller & Albrecht 2002). This translates into $\sigma_{\log L} \sim 0.02$, a much smaller error than the intrinsic scatter of GRBs. Thus, this source of uncertainty should not influence our conclusions.

Notice that we have used low-redshift GRBs from the generated sample to calibrate the relations equations (9) and (10) through a standard χ^2 fitting procedure. That is, our procedure consisted the following:

(i) generating a GRB sample;

Table 1. Values used in the calibration test.

Parameter	Value
B_v	$10^{55.32}$
β_v	1.57
σ_v	0.20
B_τ	$10^{50.03}$
β_τ	-1.27
σ_τ	0.35

Table 2. Results from calibration test. The last column refers to the uncertainty of the distance modulus determination using our method.

$N_{\rm GRB}$ used in calibration	σ_{β_τ}	σ_{β_V}	σ_μ (mag)
40	0.053	0.021	0.68
100	0.033	0.014	0.66
200	0.023	0.010	0.66

(ii) for each GRB in the sample, assigning a time-lag and variability via equations (13) and (14);

(iii) fitting the calibration relations equations (9) and (10) for the low-z GRBs from the mock sample;

(iv) repeating the steps for different size samples, and studying the precision of the attained fits.

Our results are shown in Table 2. The smaller sample size corresponds to what is expected to be found by the *Swift* satellite in its three-year campaign; the second sample size corresponds to the number of low-z GRBs that should be found if there were about 500 GRBs in total, while the third sample corresponds to about 1000 GRBs in total. It should be noted that the smaller sample represents a fourfold improvement on the sample used by Schaefer (2003).

2.4 Estimating $L_{\rm iso}$ and the χ^2 test

For the remaining GRBs that were not used in the calibration procedure, the calibrated relations are used to find $L_{\rm iso}$ from the values of τ and V. Thus, we obtain two estimates:

$$\log L_V = \log B_v + \beta_v \log V, \tag{15}$$

$$\log L_\tau = \log B_\tau + \beta_\tau \log \tau_{\rm lag}. \tag{16}$$

These two estimates are combined as weighted averages to produce one estimate of $L_{\rm iso}$:

$$\log L_{\rm iso} = \frac{1}{2} \left(\frac{1}{\sigma_{\log L_V}} \log L_V + \frac{1}{\sigma_{\log L_\tau}} \log L_\tau \right). \tag{17}$$

The next step consists of defining the χ^2 function

$$\chi^2(\boldsymbol{p}) = \sum_i^{N_{\rm GRB}} \left[\frac{m_i - M_i - 25 - 5 \log d_L(z_i, \boldsymbol{p})}{\sigma_\mu} \right]^2, \tag{18}$$

where m_i is the observed magnitude, M_i is the absolute magnitude estimated from equations (15) and (16), and $d_L(z_i, \boldsymbol{p})$ is the standard luminosity distance as function of redshift z and the cosmological parameters $\boldsymbol{p}$. The denominator σ_μ is the uncertainty in the determination of the distance modulus, $\mu = m_i - M_i$. This uncertainty was calculated using Gaussian error propagation, and assuming that

there were no correlation terms to be taken into account. The values of σ_μ we have found are shown in Table 2. We have to minimize this function and draw the χ^2 contours in order to find the confidence regions.

Here we follow the method developed for the study of SNe Ia (Goliath et al. 2001; Weller & Albrecht 2002; Di Pietro & Claeskens 2003; Silva & Bertolami 2003). We use the log-likelihood function χ^2 to build confidence regions in the parameter space. In order to perform this, we choose a fiducial model, denoted by the parameter vector $\boldsymbol{p}_{\rm fid}$, and then the log-likelihood functions χ^2 are calculated based on hypothetical magnitude measurements at the various redshifts. The χ^2 function is then given by

$$\chi^2(\boldsymbol{p}) = \sum_i^{N_{\rm GRB}} \left[\frac{5\log d_L(z_i, \boldsymbol{p}_{\rm fid}) - 5\log d_L(z_i, \boldsymbol{p})}{\sigma_\mu} \right]^2 . \quad (19)$$

Of course, there is no need to minimize the χ^2 function because its minimum will correspond to $\boldsymbol{p} = \boldsymbol{p}_{\rm fid}$; thus, we only need to find the χ^2 contours corresponding to the desired confidence level (CL).

2.5 The models

The GCG model smoothly interpolates between a dark matter dominated time in the past, to an accelerated de Sitter phase in the future. Thus, this is a setting that on large scales agrees with the observed expansion history of the Universe (Kamenshchik et al. 2001; Bento et al. 2002b). The GCG density may be written as a function of redshift as

$$\rho_{\rm ch}(z) = \rho_{\rm ch,0} \left[A_{\rm s} + (1 - A_{\rm s})(1+z)^{3(1+\alpha)} \right]^{1/(1+\alpha)} \quad (20)$$

where $\rho_{\rm ch,0}$ is the present-day density of the GCG, and

$$A_{\rm s} \equiv A\rho_{\rm ch,0}^{-(1+\alpha)}; \quad (A+B)^{1/(1+\alpha)} = \rho_{\rm ch,0}, \quad (21)$$

where B is the integration constant that appears in equation (2). For $z \gg 0$ we have a matter-dominated universe

$$\rho_{\rm ch}(z \gg 0) = (1 - A_{\rm s})^{1/(1+\alpha)}(1+z)^3, \quad (22)$$

while in the far future, $z = -1$, the GCG behaves as a vacuum-dominated universe.

The GCG unifies dark matter and dark energy, but does not take into account the presence of baryons and radiation. The baryonic component has to be considered when studying the implications of the GCG model with regard to observational tests, but for geometric tests, such as the magnitude-redshift relation we consider here, the effect of these components is negligible. Therefore, throughout the paper we disregard the presence of baryons and radiation. This does not affect any of our conclusions.

For the purpose of comparison we choose the so-called XCDM model, which consists of two components, cold dark matter and some form of dark energy which has a constant negative equation of state, $w = p/\rho$. We use this parametrization to test GRBs as a probe of an unspecified dark energy component. Although this parametrization is not suitable for general dark energy models, because in most cases the equation of state changes with time, it is adequate to test the cosmological constant model, $w = -1$, against other models. If it is found that $w = -1$ is disfavoured by the data, then there is a strong indication that the dark energy component is more complex than expected.

For many years cosmologists were mainly concerned with models to which $-1 \leqslant w < -2/3$; however, more recently mounting evidence that $w < -1$, the so-called phantom dark energy models (Caldwell 2002; Carrol, Hoffman & Trodden 2003), is being encountered. In many models there are several theoretical reasons not to consider $w < -1$, most notably that this would lead to a breakdown of the weak, the dominant and the strong energy conditions ($\rho \geqslant 0$ and $\rho + p \geqslant 0$, $\rho \geqslant |p|$, and $\rho + 3p \geqslant 0$, respectively). The weak and strong energy conditions are those to hold in proving well-known singularity theorems, while the dominant energy condition guarantees the stability of a component, such that there is no creation of energy-momentum from nothing (Hawking & Ellis 1973).

Another feature of some phantom models is that they exhibit a future blow-up of the scale factor in a finite time, often referred to as the 'big rip'. Because such a universe has a finite lifetime, it has been argued that these phantom models solve the coincidence problem; that is, they explain why dark matter and dark energy densities are of the same order at the present time. For a ΛCDM universe, a long matter-dominated period is followed by a rather quick transition to a phase such as the one the Universe is in now, where matter and dark energy have approximate densities. This phase is then followed by an eternal vacuum-dominated exponential expansion. Within this framework, the probability of finding ourselves in this intermediate and temporary epoch is very small. For phantom models, however, the accelerated expansion is not eternal. Because the Universe has a finite lifetime, the probability of living in the epoch of matter-energy approximate equality is larger than that of ΛCDM models. Thus, the cosmic coincidence is not as unlikely as for ΛCDM models. However, these models fail to explain why the dark energy component did not start to dominate the evolution at an earlier time, i.e. why dark energy started dominating the cosmic evolution only after the large-scale structure had time to evolve deep into the non-linear regime, even though in the context of the CGC this is exactly what is found (Bento et al. 2004).

Furthermore, besides these theoretical features, the latest SNe Ia data do seem to favour a phantom energy component. Thus, in what follows, we consider a phantom model for comparison with the GCG model. Moreover, as shown in Bertolami et al. (2004) and Bento et al. (2005), for $z < 2$, the GCG model is degenerate with phantom models with suitable parameters.

As mentioned, we consider two different cosmological models: the flat GCG model, which unifies dark energy and dark matter into a single component, and the XCDM, which parametrizes dark energy in terms of a constant equation of state, $w = p/\rho$. We consider that the Universe is flat in both models. The GCG model is then described by the exponent α, and the quantity $A_{\rm s}$, while the XCDM is described by the parameters w and $\Omega_{\rm m}$, the non-relativistic dark matter density relative to the critical one. We have considered two fiducial models. Model I assumes that the Universe is described by a GCG model with $1 - A_{\rm s} = 0.3$ and $\alpha = 1$. Model II assumes the corresponding degenerate Universe, described by a phantom XCDM model, with $w = -1.4$ and $\Omega_{\rm m} = 0.45$.

3 RESULTS

In Table 2 we show the estimated uncertainty in the distance modulus for each calibration. As can be observed, calibrating the luminosity estimators with just 40 low-redshift GRBs will yield a satisfactory estimate of the distance modulus. This uncertainty of $\sigma_\mu \approx 0.68$ is close to half the uncertainty found by Schaefer (2003), who used only nine GRBs to perform the calibration. Because we are dealing with a population that shows a large statistical uncertainty, increasing the number of GRBs used in the calibration will be rewarded by a smaller systematic error on the distance modulus. However, as its value is decreased, the systematic contribution to the distance modulus uncertainty will be overwhelmed by the statistical scatter

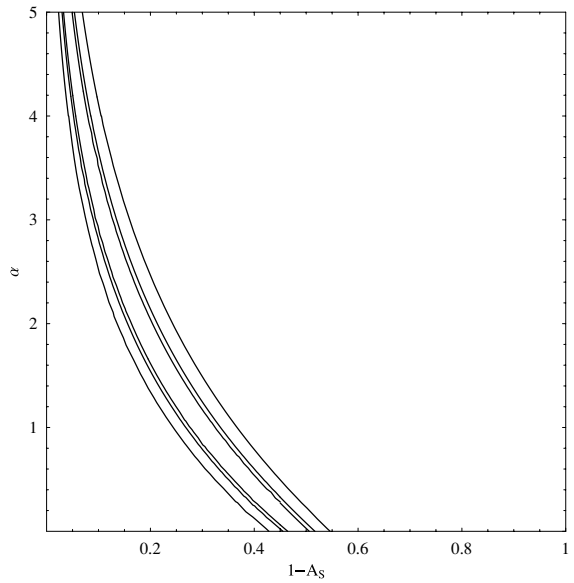

Figure 2. Confidence regions for the GCG model as a function of the number of GRBs. The curves show the 68 per cent CL regions, from the outer to the inner curves, corresponding to 150, 500 and 1000 high-redshift GRBs.

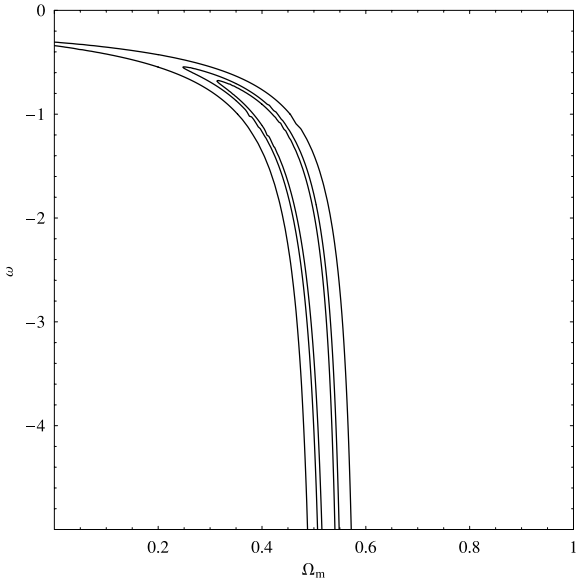

Figure 3. Confidence regions for the XCDM model as a function of the number of GRBs. The curves show the 68 per cent CL regions, from the outer to the inner curves, corresponding to 150, 500 and 1000 high-redshift GRBs.

of the population. This may be seen for the calibrations that were performed using 100 and 200 GRBs. Although the calibration precision is improved, there is little effect on σ_μ.

We then tested the effect of an increase in the number of high-redshift GRBs in the test. We assume for the purpose of calibration that 100 low-redshift GRBs are known, and use the corresponding calibration precision shown in Table 2. We next consider larger samples of GRBs. Samples with 150, 500 and 1000 high-redshift GRBs are examined, and the respective confidence regions are exhibited. These results are shown in Figs 2 and 3.

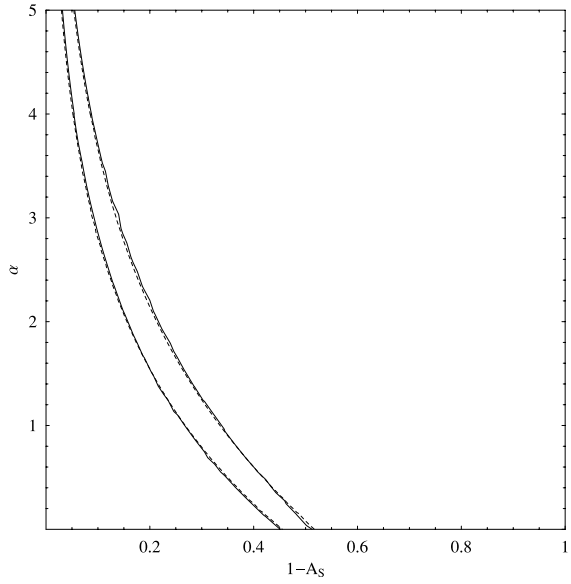

Figure 4. Confidence regions for the GCG model for two different GRBs distributions. The solid lines show the 68 per cent CL regions obtained for a sample made up of 100 low-redshift plus 400 high-redshift GRBs, while the dashed lines show the 68 per cent CL constraints for a sample made up of 500 high-redshift GRBs only. For the GCG model there is very little difference, as both curves are essentially indistinguishable.

Finally, we study the effect of the distribution of GRBs in redshift space. One of the main advantages of GRBs is that they probe a redshift range that is far beyond the possibilities of any other known standard candle such as SNe Ia. Previously we considered samples that consisted of only high-redshift GRBs to verify what could be gained by studying this redshift range exclusively. The next point to be considered is whether the loss of information at lower redshift is important. To answer this question we added 100 GRBs with $z < 1.5$ to a sample of 400 high-redshift GRBs, and found the corresponding confidence regions. It is assumed that this low-redshift sample was not used in the calibration of the luminosity indicators, thus avoiding any circularity problems. The results are shown in Figs 4 and 5.

The first conclusion we can draw is that GRBs are not quite suitable as stand-alone probes of dark energy. This is seen from the lack of impact that an increase in the redshift range has on the results in terms of precision and discriminating power.

The main source of uncertainty comes from the intrinsic statistical scatter of the GRB population. As may be seen from Table 2, calibrating the $(\tau, L_{\rm iso})$ and $(V, L_{\rm iso})$ relations with more than about 40 low-redshift GRBs does not substantially affect the results. However, an increase in the size of the higher-redshift GRB population will improve the quality of the constraints that can be imposed. This can be seen in Figs 2 and 3. Using more precise luminosity estimators, such as the one we use in the following section, might improve the outcome, even though better results can be achieved by probing a greater sample of $z < 1.5$ redshift sources. This is evident for XCDM models, as shown in Fig. 5. Adding an additional 100 GRBs with $z < 1.5$ to a sample of 400 high-redshift GRBs is more effective than adding an additional 500 GRBs with $z > 1.5$.

Regarding the results for each model, the first conclusion is that the XCDM model is better constrained than the CGC model. It can be seen that no constraint in the α parameter for the GCG model can be imposed, even though an upper limit for $A_{\rm s}$ can be obtained.

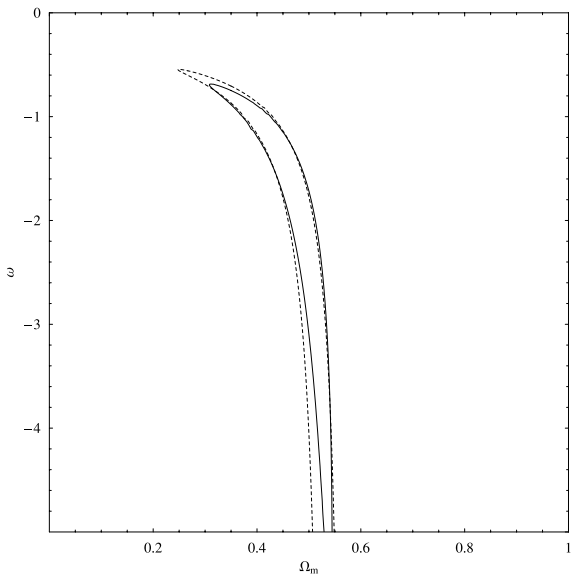

Figure 5. Confidence regions for the XCDM model for two different GRBs distributions. The solid lines show the 68 per cent CL regions obtained for a sample made up of 100 low-redshift plus 400 high-redshift GRBs, while the dashed lines show the 68 per cent CL constraints for a sample made up of 500 high-redshift GRBs only. For XCDM models, the use of some low-redshift GRBs yields a better result than using only high-redshift GRBs; however, the lower limit on the dark energy equation of state is still out of range.

As for XCDM models, we point out that there is some potential to probe $\Omega_{\rm m}$, but the prospect of using this test to probe the nature of dark energy is very limited. An upper value for w can be obtained; however, no lower limit. It should be noted that other tests such as SNe Ia are capable of imposing tighter constraints on $\Omega_{\rm m}$ than those we find, as we show later.

4 THE GHIRLANDA RELATION

4.1 Description

The (τ, $L_{\rm iso}$) and (V, $L_{\rm iso}$) relations are notoriously affected by the large intrinsic scatter of the data set, which greatly hinders their use as precision cosmological probes. Quite recently, Ghirlanda et al. (2004a) have found a surprisingly tight correlation between the peak energy of the gamma-ray spectrum, $E_{\rm peak}$ (in the ν–νF_ν plot), and the collimation corrected energy emitted in gamma-rays, E_γ, for long GRBs. This collimation corrected energy measures the energy release by the GRB taking into account that the energy is beamed into a jet with aperture angle θ.

Let us denote by $E_{\rm iso}$ the isotropically equivalent energy, inferred from the isotropic GRB emission. This source frame 'bolometric' isotropic energy is found by integrating the best-fitting time-integrated spectrum $N(E)$ (photons cm^{-2} keV^{-1}) over the energy range 1–10 MeV:

$$E_{\rm iso} = \frac{4\pi d_L^2(z)}{1+z} S_\gamma k \quad \text{erg}. \tag{23}$$

Here, $d_L(z)$ is the GRB luminosity distance, k refers to the k-correction (Bloom, Frail & Sari 2001) and S_γ is the fluence

$$S_\gamma = \int_1^{10^4} E N(E)\,{\rm d}E, \tag{24}$$

where E is in keV.

If the gamma-ray emission is collimated into a jet with aperture θ, then the true energy emitted is $E_\gamma = E_{\rm iso}(1-\cos\theta)$. Thus, to convert $E_{\rm iso}$ into E_γ and vice versa, we need to know the angle θ. Under the simplifying assumption of a constant circum-burst density medium of number density n, a fireball emitting a fraction η_γ of its kinetic energy in the prompt gamma-ray phase would show a break in its afterglow light curve when its bulk Lorentz factor Γ becomes of the order of $\Gamma \simeq 1/\theta$, with θ given by (Sari 1999)

$$\theta = 0.161 \left(\frac{t_{\rm jet}}{1+z}\right)^{3/8} \left(\frac{n\eta_\gamma}{E_{\rm iso,52}}\right)^{1/8} \tag{25}$$

where $t_{\rm jet}$ is the break time in d, and $E_{\rm iso,52} = E_{\rm iso}/10^{52}$ erg.

The Ghirlanda relation (Ghirlanda et al. 2004a; Xu 2005) is then expressed as

$$\frac{E_\gamma}{10^{50}\,{\rm erg}} = C \left(\frac{E_{\rm p}}{100\,{\rm keV}}\right)^a \tag{26}$$

where a and C are dimensionless parameters.

Using this result, together with equations (23), (25) and the definition of E_γ, we obtain an equation for $d_L(z)$

$$C \left(\frac{E_{\rm p}}{100\,{\rm keV}}\right)^a = (1-\cos\theta)\left(\frac{E_{\rm iso}}{10^{50}\,{\rm erg}}\right). \tag{27}$$

Note that both $E_{\rm iso}$ and θ depend on $d_L(x)$, as may be seen from their definitions. Solving this equation for $d_L(z)$ we find an estimate of the luminosity distance at redshift z in terms of the observables $E_{\rm p}$, $t_{\rm jet}$, n, and fluence S_γ.

The error budget for d_L is then found to be (Xu 2005)

$$\begin{aligned}\left(\frac{\sigma_{d_L}}{d_L}\right)^2 = {} & \frac{1}{4}\left[\left(\frac{\sigma_{S_\gamma}}{S_\gamma}\right)^2 + \left(\frac{\sigma_k}{k}\right)^2\right] + \frac{1}{4}\frac{1}{(1-\sqrt{C_\theta})^2} \\ & \times \left[\left(\frac{\sigma_C}{C}\right)^2 + \left(a\frac{\sigma_{E_{\rm p}^{\rm obs}}}{E_{\rm p}^{\rm obs}}\right)^2 + \left(a\frac{\sigma_a}{a}\ln\frac{E_{\rm p}}{100}\right)^2\right] \\ & + \left\{\left(\frac{3\sigma_{t_j}}{t_j}\right)^2 + \left(\frac{\sigma_{n_0}}{n_0}\right)^2 + \left[\frac{\sigma_{\eta_\gamma}}{\eta_\gamma(1-\eta_\gamma)}\right]^2\right\} \\ & \times \frac{1}{4}\frac{C_\theta}{(1-\sqrt{C_\theta})^2},\end{aligned} \tag{28}$$

where $C_\theta^2 = \theta\sin\theta/(8-8\cos\theta)$.

The distance modulus is given by $\mu_{\rm obs} = 5\log d_L/10\,{\rm pc}$, and thus its error is $\sigma_\mu = 5/\ln 5\,(\sigma_d L/d_L)$. We use the error estimates from Xu (2005), which are consistent with what is found in the literature (Ghirlanda et al. 2004a,b; Friedman & Bloom 2005b; Ghisellini et al. 2005; Mörtsell & Sollerman 2005; Xu, Dai & Liang 2005).

These values yield an uncertainty in $\mu_{\rm obs}$ of the order of $\sigma_\mu \simeq 0.5$, which is just slightly smaller than the error bars from using both the ($L_{\rm iso}$, V) and ($L_{\rm iso}$, τ_L) relations. As can be observed in Table 3, the smaller intrinsic scatter of the Ghirlanda relation is balanced by its dependence on poorly constrained quantities. Improving the calibration will not solve the problem, because the main sources of uncertainty are a result of the determination of the peak energy $E_{\rm p}$, the jet break time $t_{\rm jet}$ and the value of the circum-burst density n. The determination of $t_{\rm jet}$ will become much more precise in the near future thanks to *Swift*, but unfortunately the relatively narrow spectral range of *Swift* will greatly hinder the determination of $E_{\rm p}$ (Friedman & Bloom 2005b). Using additional data from the *High-Energy Transient Explorer II* (*HETE II*) experiment may reduce this uncertainty thanks to its larger bandpass of [30, 400] keV (compared to the [15, 150] keV bandpass of *Swift*).

Table 3. Error budget for the Ghirlanda test. The uncertainty in the circumburst density is assumed to be 50 per cent, while the other values are taken from Xu (2005).

	Error (per cent)	Contribution to $(\sigma_{d_l}/d_l)^2$	Percentage of $(\sigma_{d_l}/d_l)^2$ (per cent)
$(\sigma_{S_\gamma}/S_\gamma)^2$	10	0.0027	5
$(\sigma_k/k)^2$	5	0.0006	1
$(\sigma_C/C)^2$	8	0.0027	5
$(\sigma_a/a)^2$	5	0.0025	5
$(\sigma_{E_\mathrm{p}}/E_\mathrm{p})^2$	17	0.0259	52
$(\sigma_n/n)^2$	50	0.0069	14
$(\sigma_{t_\mathrm{jet}}/t_\mathrm{jet})^2$	20	0.0081	16

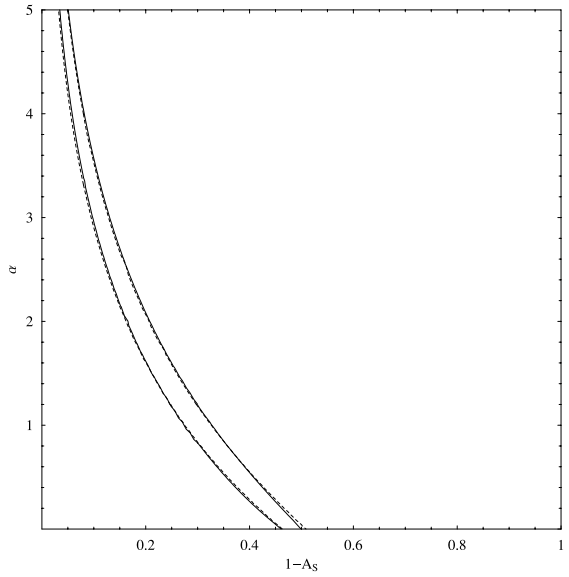

Figure 6. Confidence regions found for the GCG model using the Ghirlanda relation. The solid lines show the 68 per cent CL regions obtained for a sample made up of 100 low-redshift plus 400 high-redshift GRBs, while the dashed lines show the 68 per cent CL constraints for a sample made up of 500 high-redshift GRBs only. For the GCG model, we cannot place limits on α, and only very loose ones on A_s.

4.2 Results

In Figs 6 and 7 we see the improvements that can be obtained by the use of the Ghirlanda relation. We have assumed two redshift distributions: one made up of 500 GRBs with $z > 1.5$, and the other made up of 100 GRBs with $z < 1.5$ plus 400 GRBs with $z > 1.5$, as before. For the CGC model we find that the conclusions that can be drawn remain essentially unchanged. It is obvious that the high redshifts of GRBs are not quite suitable to adequately study the GCG model.

Regarding the XCDM model, a rather useful limit to the total amount of matter may be imposed, but the use of some low-redshift GRBs is fundamental to constrain the dark energy equation of state. However, even with these low-redshift GRBs, the uncertainty on w is still large, especially when compared to SNe Ia.

4.3 Joint constraints from SNe Ia and GRBs

Finally, we have studied whether GRBs might improve the results provided by SNe Ia. Because we are considering future GRB surveys, we use the *SNAP* experiment as the SNe Ia benchmark. We

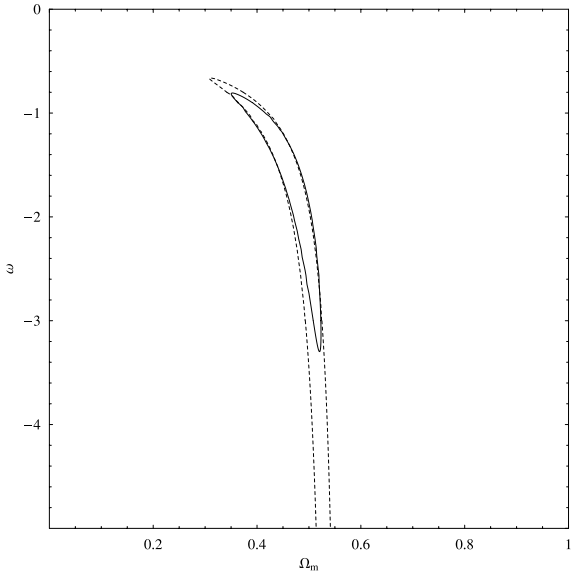

Figure 7. Confidence regions found for the XCDM model using the Ghirlanda relation. The solid lines show the 68 per cent CL regions obtained for a sample made up of 100 low-redshift plus 400 high-redshift GRBs, while the dashed lines show the 68 per cent CL constraints for a sample made up of 500 high-redshift GRBs only. The increase in precision does not greatly alter the allowed parameter range when high-redshift GRBs are used exclusively, but when some information on the $z \leqslant 1.5$ region is used, the constraints on w improve considerably.

built the expected confidence regions for *SNAP* using the method discussed in Silva & Bertolami (2003) and Bertolami et al. (2004), and then built joint confidence regions for *SNAP* and GRBs. We choose to marginalize over the unwanted parameter $\mathcal{M}$ (Goliath et al. 2001). We considered the use of the Ghirlanda relation on a sample comprising 500 high-redshift GRBs. The results are shown in Figs 8 and 9.

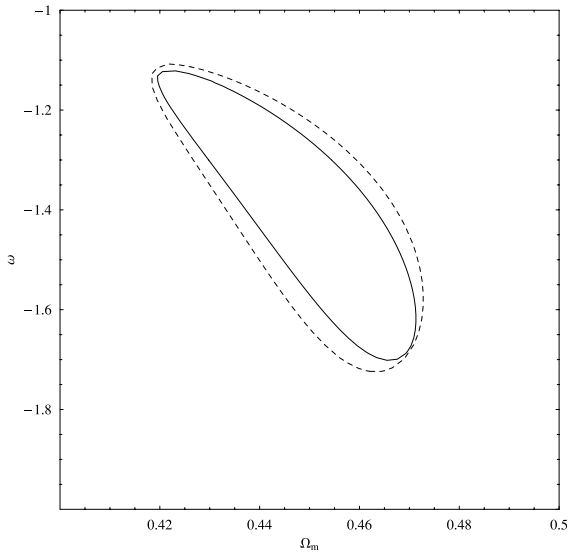

Figure 8. Joint constraints from *SNAP* plus 500 high-redshift GRBs for an XCDM model. The dashed line corresponds only to *SNAP* constraints, while the solid region corresponds to the *SNAP*+GRB constraints. All curves correspond to the 68 per cent CL. Notice that an improvement, although marginal, is obtained.

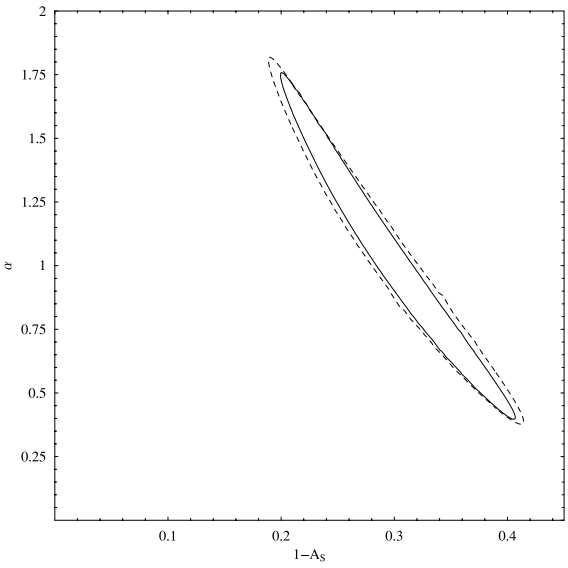

Figure 9. Joint constraints from *SNAP* plus 500 high-redshift GRBs for a GCG model. The dashed line corresponds only to *SNAP* constraints, while the solid region corresponds to the *SNAP*+GRB constraints. All curves correspond to the 68 per cent CL. Only a marginal improvement is observed.

The use of GRBs will produce a quite modest improvement relative to the *SNAP* result. In fact, we find that the uncertainty on the distance modulus determined by GRBs would have to decrease by a factor of 2 or more in order that GRBs improve *SNAP* allowed regions noticeably.

In favour of GRBs though, it should be noted that if a large GRB sample becomes available before the *SNAP* data, GRBs might improve SNe Ia constraints, as the SNe constraints will not be as precise as those expected for *SNAP*. This is especially true for XCDM models, where, as we have mentioned above, GRBs are expected to provide a fair and independent constraint on $\Omega_{\rm m}$. Still, it should be noted that available SNe Ia data place limits on $\Omega_{\rm m}$ that are close to those predicted here (Tonry et al. 2003; Choudhury & Padmanabhan 2005). Thus, it seems likely that GRBs will eventually play more the role of a consistency test than a tool of precision cosmology.

5 DEGENERACY BETWEEN MODELS

The CGC and the phantom XCDM models are degenerate at redshifts $z < 2$, as shown in Bertolami et al. (2004) and Bento et al. (2005). Consider the Taylor expansion of the luminosity distance up to the fourth power of redshift (Visser 2004):

$$d_L = \frac{c}{H_0}\left\{ z + \frac{1}{2}(1-q_0)z^2 - \frac{1}{6}\left(1 - q_0 - 3q_0^2 + j_0\right) z^3 + \frac{1}{24}\left[2 - 2q_0 - 15q_0^2 - 15q_0^3 + 5j_0 + 10q_0 j_0 + k_0\right] \times z^4 + O(z^5)\right\}. \quad (29)$$

Here, q_0 is the deceleration parameter, related to the second derivative of the expansion factor, j_0 is the so-called 'jerk' or state finder parameter (Alam et al. 2003; Sahni et al. 2003), related to the third derivative of the expansion factor, and k_0 is the so-called 'kerk' parameter, which is related to the fourth derivative of the expansion parameter (Dabrowski & Stachowiak 2004; Visser 2004), all evaluated at present. These quantities are defined as

$$q(t) = -\frac{1}{a}\frac{{\rm d}^2 a}{{\rm d}t^2}\left(\frac{1}{a}\frac{{\rm d}a}{{\rm d}t}\right)^{-2}, \quad (30)$$

$$j(t) = +\frac{1}{a}\frac{{\rm d}^3 a}{{\rm d}t^3}\left(\frac{1}{a}\frac{{\rm d}a}{{\rm d}t}\right)^{-3}, \quad (31)$$

$$k(t) = +\frac{1}{a}\frac{{\rm d}^4 a}{{\rm d}t^4}\left(\frac{1}{a}\frac{{\rm d}a}{{\rm d}t}\right)^{-4}. \quad (32)$$

These are related to each other through the relations

$$q(z) = \frac{3}{2}\left[\frac{p(z)}{\rho(z)} + 1\right] - 1, \quad (33)$$

$$j(z) = q(z) + 2q^2(z) + (1+z)\frac{{\rm d}q}{{\rm d}z}(z), \quad (34)$$

$$k(z) = -(1+z)\frac{{\rm d}j}{{\rm d}z}(z) - 2j(z) - 3j(z)q(z), \quad (35)$$

where $\rho(z)$ and $p(z)$ refer to the total density and pressure of the Universe, respectively. With these expressions it is possible to write the present-day values of the parameters as a function of the cosmological parameters of the model under examination.

For the XCDM model, we have

$$q_0^{\rm XCDM} = \frac{3}{2}\left[1 + w(1-\Omega_{\rm m})\right] - 1, \quad (36)$$

$$\left.\frac{{\rm d}q}{{\rm d}z}\right|_0^{\rm XCDM} = \frac{9}{2}w^2(1-\Omega_{\rm m})\Omega_{\rm m}, \quad (37)$$

$$\left.\frac{{\rm d}j}{{\rm d}z}\right|_0^{\rm XCDM} = -\frac{27}{2}w^2(1+w)(\Omega_{\rm m}-1)\Omega_{\rm m}, \quad (38)$$

while for the GCG model we find

$$q_0^{\rm GCG} = \frac{3}{2}(1-A_{\rm s}) - 1, \quad (39)$$

$$\left.\frac{{\rm d}q}{{\rm d}z}\right|_0^{\rm GCG} = \frac{9}{2}A_{\rm s}(1-A_{\rm s})(1+\alpha), \quad (40)$$

$$\left.\frac{{\rm d}j}{{\rm d}z}\right|_0^{\rm GCG} = -\frac{27}{2}(1+\alpha)\alpha(A_{\rm s}-1)(2A_{\rm s}-1)A_{\rm s}. \quad (41)$$

For the redshift range probed by SNe Ia we can neglect terms beyond the cubic power in redshift in equation (29). SNe Ia data indicate that these models have the same deceleration and jerk (Bertolami et al. 2004; Bento et al. 2005), i.e. they are degenerate for the considered redshift range. Thus, imposing this equality we find the relationship between parameters

$$w = \alpha(A_{\rm s}-1) - 1, \quad (42)$$

$$\Omega_{\rm m} = \frac{(1+\alpha)(1-A_{\rm s})}{1+\alpha(1-A_{\rm s})}. \quad (43)$$

This degeneracy holds for SNe Ia, for the maximum probed redshift of about $z \approx 2$. As the redshift range allowed by GRBs is greater, we hope to test higher-order terms in equation (29). At the next order, the degeneracy is broken by the kerk parameter; that is, even if $q_0^{\rm GCG} = q_0^{\rm XCDM}$, $j_0^{\rm GCG} = j_0^{\rm XCDM}$, we find that $k_0^{\rm GCG} \neq k_0^{\rm XCDM}$. For instance, if we consider $\alpha = 1$ and $A_{\rm s} = 0.7$, then $k_0^{\rm GCG} = -0.68$, while for the corresponding XCDM model (with $w = -1.3$ and $\Omega_{\rm m} = 0.46$), the kerk is $k_0^{\rm XCDM} = 1.02$.

This procedure can be viewed as a consistency test. Indeed, consider the GCG model. Once the deceleration, the jerk and the kerk of the Universe are measured, we can extract the values of α and $A_{\rm s}$. These values yield a value for the kerk, called $k_0^{\rm t}$, which can be compared to the measured value of the kerk, $k_0^{\rm m}$. Whether both values are close or not, we can reach a conclusion regarding the suitability of the model. The same reasoning can be applied to the XCDM model. This is, of course, a simplification, because we have to consider the accuracy of measurements and the statistical significance of each of the parameters in equation (29), as well as considering correlations between them.

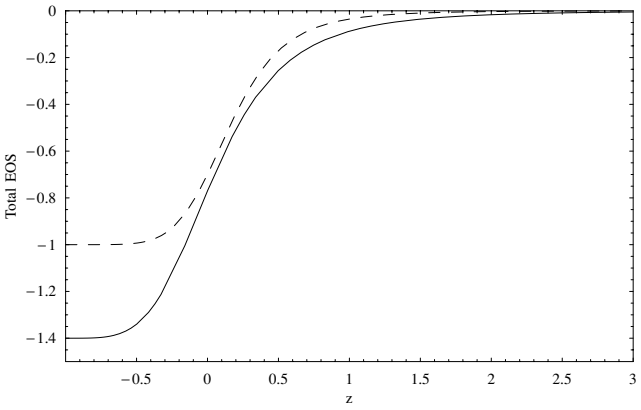

Figure 10. Total equation of state of the Universe as a function of redshift. The value $z = -1$ corresponds to the very far future. The dashed line represents our GCG fiducial model, while the solid line corresponds to the XCDM phantom model.

6 DISCUSSION AND CONCLUSIONS

We have verified that the medium and high redshifts of GRBs do not impose too strong constraints on the GCG model. At such high redshifts, the expansion factor for the GCG becomes

$$H_{\rm ch}(z \gg 0) = \Omega_{\rm ch}(1 - A_{\rm s})^{1/(1+\alpha)}(1 + z)^3 \qquad (44)$$

where $\Omega_{\rm ch}$ is the CGC density relative to the critical one. Because we are considering a flat universe made up mostly by the GCG, $\Omega_{\rm ch} = 1$. Thus, the luminosity distance at such high redshifts depends essentially on $(1 - A_{\rm s})^{1/(1+\alpha)}$. It is found that the confidence regions for the GCG model approximately follow the line $(1 - A_{\rm s})^{1/(1+\alpha)} =$ const. Hence, because $A_{\rm s}$ and α are strongly correlated by this expression, neither one is constrained.

As for the XCDM model, a high-redshift population of GRBs is suitable to constrain the total amount of matter, $\Omega_{\rm m}$, but such high-redshift GRBs are poor probes of the dark energy equation of state. This does not mean that GRBs have no use for the study of dark energy, or that expanding the Hubble diagram is meaningless. It is a common trend in the recent literature to argue that a precise prior estimate of $\Omega_{\rm m}$ enhances the ability of SNe Ia to constrain the dark energy equation of state (Goliath et al. 2001; Weller & Albrecht 2002; Di Pietro & Claeskens 2003). Our results are in complete agreement with these studies (Dai, Liang & Xu 2004; Ghirlanda et al. 2004b; Friedman & Bloom 2005a,b; Ghisellini et al. 2005; Mörtsell & Sollerman 2005; Xu et al. 2005; Xu 2005).

For GRBs, a tight constraint on $\Omega_{\rm m}$ is also important to study the equation of state parameter w. A high-redshift sample will constrain $\Omega_{\rm m}$, while a low-redshift sample will place constraints on the equation of state. However, we have verified that a low-redshift sample alone will fail to constrain the equation of state, because it will be hindered by large uncertainties in $\Omega_{\rm m}$. This is somewhat similar to what happens in SNe Ia tests. A low-redshift sample will constrain the parameter $\mathcal{M}$, while the high-redshift sample constrains the cosmological parameters (Padmanabhan & Choudhury 2003; Choudhury & Padmanabhan 2005). Thus, we conclude that while the use of high-redshift GRBs will allow probing the dark matter component, to study the nature of dark energy, a low-redshift probe is necessary. We could of course use GRBs, but for the $z < 1.5$ range, SNe Ia are the natural choice because of their precision.

Our study also reveals that the effectiveness of the GRB test depends on the model under examination. GRBs allow us to impose some constraints on the XCDM model, but very little can be extracted for the GCG model. This may be explained by two factors. The first has been explained above, and is related to the fact that the region probed by GRBs depends on a unique function of both parameters. The second is related to how late the Universe stops being matter-dominated. As shown in Fig. 10, the CGC model remains in the matter-dominated phase for a longer time, and thus the period of time during which the dark energy behaviour affects the cosmic expansion is slightly larger for the XCDM model. Because GRBs essentially probe larger redshifts, models in which the transition between the matter-dominated and accelerated expansion is shorter cannot be well constrained by this test. By the same reasoning, GRBs might actually be useful in testing models where the transition between matter-dominated expansion and dark energy driven acceleration started at larger redshifts. In general, we expect that GRBs are particularly suited to study models that depart from the ΛCDM behaviour at larger redshifts.

Thus, we find that despite all intrinsic limitations, larger samples of GRBs can potentially determine the total amount of matter in a XCDM model. This independent determination of $\Omega_{\rm m}$ will be useful in studies of the dark energy equation of state, at least until *SNAP* becomes a reality. If *SNAP* provides the scientific bounty it promises, then GRBs can be regarded as a consistency test. On the run up to *SNAP* though, constraints imposed by GRBs may become quite helpful in studies of dark energy.

Furthermore, GRBs may also be used to break the degeneracy between models, because at high redshifts the effect of higher-order terms in the Taylor expansion of $d_L(z)$ must be taken into account.

Naturally, a word of caution on the proposed methodology is in order though, as very little is known about the physics behind the correlations used. The $L_{\rm iso}$–τ and $L_{\rm iso}$–V relations are purely phenomenological, and no well-established explanation exists, although some tentative explanations have been put forward (see Ioka & Nakamura 2001; Plaga 2001; Schaefer 2004). The situation for the Ghirlanda relation is more complex, as this correlation depends on poorly constrained quantities, such as the circum-burst density n, and the gamma-ray creation efficiency, η_γ, and a model of the jet structure must be assumed. Also, as noted by Levinson & Eichler (2005), the beaming correction appears to be biased because of the fact that the inferred opening angle depends on $E_{\rm iso}$ (see equation 25). Furthermore, several other systematic effects have yet to be considered, namely selection effects (Band & Preece 2005; Nakar

& Piran 2005) as well as gravitational lensing and other effects (Friedman & Bloom 2005a).

REFERENCES

Alam U., Sahni V., Saini T. D., Starobinsky A. A., 2003, MNRAS, 344, 1057
Albrecht A., Skordis C., 2000, Phys. Rev. Lett., 84, 2076
Alcaniz J. S., Jain D., Dev A., 2003, Phys. Rev. D, 67, 043514.
Amendola L., 1999, Phys. Rev. D, 60, 043501
Amendola L., Finelli F., Burigana C., Carturan D., 2003, J. Cosmol. Astropart. Phys., 07, 005
Band D. L., Preece R. D., 2005, ApJ, 627, 319
Band D. et al., 1993, ApJ, 413, 281
Barris B. J. et al., 2004, ApJ, 602, 571
Bento M. C., Bertolami O., 1999, Gen. Relat. Gravitation, 31, 1461
Bento M. C., Bertolami O., Silva P. T., 2001, Phys. Lett. B, 498, 62
Bento M. C., Bertolami O., Santos N. C., 2002a, Phys. Rev. D, 65, 067301
Bento M. C., Bertolami O., Sen A. A., 2002b, Phys. Rev. D, 66, 043507
Bento M. C., Bertolami O., Sen A. A., 2003a, Phys. Lett. B, 575, 172
Bento M. C., Bertolami O., Sen A. A., 2003b, Phys. Rev. D, 67, 063003
Bento M. C., Bertolami O., Sen A. A., 2003c, Gen. Relat. Gravitation, 35, 2063
Bento M. C., Bertolami O., Sen A. A., 2004, Phys. Rev. D, 70, 083519
Bento M. C., Bertolami O., Santos N. M. C., Sen A. A., 2005, Phys. Rev. D, 71, 063501
Bertolami O., 1986a, Il Nuovo Cim., 93B, 36
Bertolami O., 1986b, Fortschr. Phys., 34, 829
Bertolami O., 2004, preprint (astro-ph/0403310)
Bertolami O., 2005, preprint (astro-ph/0504275)
Bertolami O., Martins P. J., 2000, Phys. Rev. D, 61, 064007
Bertolami O., Sen A. A., Sen S., Silva P. T., 2004, MNRAS, 353, 329
Bilic N., Tupper G. B., Viollier R. D., 2002, Phys. Lett. B, 535, 17
Binétruy P., 1999, Phys. Rev. D, 60, 063502
Bloom J. S., Frail D. A., Sari R., 2001, AJ, 121, 2879
Bordemann M., Hoppe J., 1993, Phys. Lett. B, 317, 315
Bronstein M., 1933, Phys. Zeit. Sowejt Union, 3, 73
Caldwell R. R., 2002, Phys. Lett. B, 545, 23
Caldwell R. R., Dave R., Steinhardt P. J., 1998, Phys. Rev. Lett., 80, 1582
Carroll S. M., Hoffman M., Trodden M., 2003, Phys. Rev. D, 68, 023509
Carturan D., Finelli F., 2003, Phys. Rev. D, 68, 103501
Chiba T., 1999, Phys. Rev. D, 60, 083508
Choudhury T. R., Padmanabhan T., 2005, A&A, 429, 807
Dabrowski M. P., Stachowiak T., 2004, preprint (hep-th/0411199)
Dai Z. G., Liang E. W., Xu D., 2004, ApJ, 612, L101
Dev A., Alcaniz J. S., Jain D., 2003, Phys. Rev. D, 67, 023515
Dev A., Jain D., Alcaniz J. S., 2004, A&A, 417, 847
Di Pietro E., Claeskens J. F., 2003, MNRAS, 341, 1299
Fabris J. C., Gonçalves S. B. V., de Souza P. E., 2002a, preprint (astro-ph/0207430)
Fabris J. C., Gonçalves S. B. V., de Souza P. E., 2002b, Gen. Relat. Gravitation, 34, 2111
Ferreira P. G., Joyce M., 1998, Phys. Rev. D, 58, 023503
Friedman A. S., Bloom J. S., 2005a, ApJ, 627, 1
Friedman A. S., Bloom J. S., 2005b, Il Nuovo Cim., in press (astro-ph/0502559)
Frolov A., Kofman L., Starobinsky A., 2002, Phys. Lett. B, 545, 8
Ghirlanda G., Ghisellini G., Lazzati D., 2004a, ApJ, 616, 331
Ghirlanda G., Ghisellini G., Lazzati D., Firmani C., 2004b, ApJ, 613, L13
Ghisellini G., Ghirlanda G., Firmani C., Lazzati D., Avila-Reese V., 2005, Il Nuovo Cim., in press (astro-ph/0504306)
Goliath M., Amanullah R., Astier P., Goobar A., Pain R., 2001, A&A, 380, 6
Gorini V., Kamenshchik A., Moschella U., 2003, Phys. Rev. D, 67, 063509
Hawking S. W., Ellis G. F. R., 1973, The Large Scale Structure Of Space–Time. Cambridge Univ. Press, Cambridge
Huterer D., Turner M. S., 2001, Phys. Rev. D, 64, 123527
Ioka K., Nakamura T., 2001, ApJ, 554, L163
Jackiw R., Polychronakos A. P., 2000, Phys. Rev. D, 62, 085019
Kamenshchik A., Moschella U., Pasquier V., 2000, Phys. Lett. B, 487, 7
Kamenshchik A., Moschella U., Pasquier V., 2001, Phys. Lett. B, 511, 265
Kim J. E., 2000, J. High Energy Phys., 0006, 016
Lamb D. Q., Reichart D. E., 2000, ApJ, 536, 1
Levinson A., Eichler D., 2005, ApJ, 629, L13
Makler M., de Oliveira S. Q., Waga I., 2003, Phys. Lett. B, 555, 1
Mörtsell E., Sollerman J., 2005, J. Cosmol. Astropart. Phys., 06, 009
Nakar E., Piran T., 2005, MNRAS, 360, 73
Norris J. P., Marani G. F., Bonnell J. T., 2000, ApJ, 534, 248
Ozer M., Taha M. O., 1987, Nucl. Phys. B, 287, 776
Padmanabhan T., Choudhury T. R., 2003, MNRAS, 344, 823
Plaga R., 2001, A&A, 370, 351
Porciani C., Madau P., 2001, ApJ, 548, 522
Press W. H., Teukolsky S. A., Vetterling W. T., Flannery B. P., 1992, Numerical Recipes in C. Cambridge Univ. Press, Cambridge
Ratra B., Peebles P. J. E., 1988a, Phys. Rev. D, 37, 3406
Ratra B., Peebles P. J. E., 1988b, ApJ, 325, L117
Reichart D. E., Lamb D. Q., Fenimore E. E., Ramirez-Ruiz E., Cline T. L., Hurley K., 2001, ApJ, 552, 57
Riess A. G. et al. (Supernova Search Team Collaboration), 2004, ApJ, 607, 665
Sahni V., Saini T. D., Starobinsky A. A., Alam U., 2003, JETP Lett., 77, 201
Sandvik H., Tegmark M., Zaldarriaga M., Waga I., 2004, Phys. Rev. D, 69, 123524
Sari R., 1999, ApJ, 524, L43
Schaefer B. E., 2003, ApJ, 583, L67
Schaefer B. E., 2004, ApJ, 602, 306
Sen A. A., Sen S., 2001, Mod. Phys. Lett., A16, 1303
Sen A. A., Sen S., Sethi S., 2001, Phys. Rev. D, 63, 107501
Silva P. T., Bertolami O., 2003, ApJ, 599, 829
Steidel C. C., Adelberger K. L., Giavalisco M., Dickinson M., Pettini M., 1999, ApJ, 519, 1
Takahashi K., Oguri M., Kotake K., Ohno H., 2003, preprint (astro-ph/0305260)
Tonry J. L. et al., 2003, ApJ, 594, 1
Uzan J. P., 1999, Phys. Rev. D, 59, 123510
Visser M., 2004, Class. Quant. Grav., 21, 2603
Weller J., Albrecht A., 2002, Phys. Rev. D, 65, 103512
Wetterich C., 1988, Nucl. Phys. B, 302, 668
Xu D., 2005, preprint (astro-ph/0504052 v1)
Xu D., Dai Z. G., Liang E. W., 2005, ApJ, 633, 603
Zhu Z-H., 2004, A&A, 423, 421
Zlatev I., Wang L., Steinhardt P. J., 1999, Phys. Rev. Lett., 82, 869

This paper has been typeset from a TEX/LATEX file prepared by the author.